J Inorg Organomet Polym (2013) 23:690–702
DOI 10.1007/s10904-013-9835-8

Electrical Properties of Triethylene Glycol Stabilized $Mn_xCo_{1-x}Fe_2O_4$ Nanoparticles

Hamit Erdemi · Ayşe Demir · Abdulhadi Baykal

Received: 30 November 2012 / Accepted: 25 January 2013 / Published online: 13 February 2013

Abstract We reported on the synthesis and analysis of the composition, micro-structure, ac–dc conductivity performance and dielectric permittivity of triethylene glycol (TEG) stabilized $Mn_xCo_{1-x}Fe_2O_4$ nanoparticles obtained by polyol method. Crystallite size from XRD and particle size from TEM micrographs are consistent with each other. Conductivity measurements were performed to investigate the influence of the coating with TEG on the conduction characteristics of $Mn_xCo_{1-x}Fe_2O_4$ NP's. The frequency-dependency of the ac conductivity shows electrode polarization effect. The dc conductivity is strongly temperature dependent and shows maximum conductivity of about 5×10^{-5} S cm^{-1} for $x = 1.0$ at 120 °C. Analysis of dielectric permittivity functions suggests that ionic and polymer segmental motions are strongly coupled.

Keywords Magnetic nanomaterials · Electrical properties · Dielectric permittivity · Conductivity · Spinels

1 Introduction

There is a great attention on the preparation and characterization of super paramagnetic metal oxide nanoparticles of spinel ferrites, MFe_2O_4 (M=Co, Mg, Mn, Ni, etc.) [1–5] due to their applications in several important technological fields such as ferrofluids, magnetic drug delivery, high density information storage [6]. It is showed that manganese substituted cobalt ferrites are excellent candidates for stress sensors due to a large magneto mechanical effect and high sensitivity to stress [7, 8].

To synthesize high quality magnetic NP's, thermal decomposition method has been considered as one of the most effective method [9, 10]. However, for the synthesis of water soluble magnetic NP's, novel thermal decomposition route is required which is called as glycothermal route. Polyol process [11, 12] is a versatile chemical approach, which refers to the use of polyols (for example ethylene glycol, diethylene glycol) to reduce metal salts to metal particles, that has successfully been used to prepare a great variety of inorganic compounds non-aggregated particles. In this method, polyol often serves as high-boiling solvent and reducing agent as well as stabilizer to control the particles growth and prevent interparticle aggregation. The advantage of this approach is the possibility to kinetically control the experimental conditions and to scale-up easily. Recently, Caruntu and co-workers [13] have prepared magnetite nanocrystals by hydrolysis of a stoichiometric ratio of $FeCl_3{\cdot}6H_2O$, $FeCl_2{\cdot}4H_2O$ and NaOH in diethylene glycol. Cai and Wan [11] demonstrated the reaction of $Fe(acac)_3$ in TEG leading to non-agglomerated and uniform magnetite particles which is most likely correlated with the appropriate number of coordinating groups available on the polyol solvent molecules [14] and the suitable reaction temperature. In this

---

H. Erdemi
Department of Polymer Engineering, Yalova University,
77100 Yalova, Turkey

A. Demir · A. Baykal (✉)
Department of Chemistry, Fatih University,
34500 B. Cekmece, Istanbul, Turkey
e-mail: hbaykal@fatih.edu.tr

A. Demir
Department of Chemistry, Istanbul Medeniyet University,
Goztepe, Istanbul, Turkey

study, water soluble triethylene glycol (TEG) was used as high boiling point solvent. The TEG solvent used can serve as a stabilizer to control the particle growth and to prevent the aggregation of particles in high temperature reaction medium. This approach has several advantages compared to other synthesis methods. First, only metal precursors were used and no further reducing agent and surfactants are required. Second, the surface of $Mn_xCo_{1-x}Fe_2O_4$ NP's were coated by hydrophilic polyol ligands insitu, and the hydrophilic property of TEG made as-prepared nanoparticles easily dispersed in water and other polar solvents. Finally, the size distribution of the nanoparticles is much narrower than those particles produced from traditional methods. Therefore this approach offers a facile route to replace the traditional co-precipitation method for the preparation of super-paramagnetic water-soluble magnetic nanoparticles and is expected to be applicable in various biomedical applications.

In this paper, we introduce the preparation and characterization of triethylene glycol stabilized $Mn_xCo_{1-x}Fe_2O_4$ nanoparticles by polyol method. To the best of our knowledge, no work has been published so far related with this nanocomposite. The structure, morphology, and the electrical properties of the nanocomposite have been characterized by means of XRD, FT-IR, TGA, TEM, dielectric impedance analyzer respectively.

2 Experimental

2.1 Materials and Instrumentations

$Mn(acac)_2$, $Co(acac)_2$, $Fe(acac)_3$ and Triethylene glycol (TEG) were obtained from Merck. All these reagents were used without further purification.

X-ray powder diffraction (XRD) analysis was conducted on a Rigaku Smart Lab Diffractometer operated at 40 kV and 35 mA using Cu K_α radiation.

Transmission electron microscopy (TEM) analysis was performed using a FEI Tecnai G2 Sphera microscope. A drop of diluted sample in alcohol was dripped on a TEM grid.

Fourier transform infrared (FT-IR) spectra of the samples were recorded with a Perkin Elmer BX FT-IR infrared spectrometer in the range of 4,000–400 cm^{-1}.

The real (ε') and imaginary (ε'') parts of complex dielectric permittivity $\varepsilon^*[=\varepsilon'(\omega)+i\varepsilon''(\omega)]$ were measured with a Novocontrol dielectric-impedance analyzer. The dielectric data (ε', ε'') were collected as a function of temperature and frequency. These films were sandwiched between gold blocking electrodes and the conductivities were measured in the frequency range of 0.1 Hz to 3 MHz at 10 °C intervals. The temperature change was controlled with a Novocontrol cryosystem with a precision of 0.01 °C.

2.2 Procedure

A stoichiometric amount of $Co(acac)_2$, $Mn(acac)_2$ and $Fe(acac)_3$ dissolved in TEG (20 ml) and then it was heated to 110 °C under vigorous magnetic stirring and nitrogen atmosphere. After heating for 1 h, the solution temperature was raised to 210 °C and kept for 2 h at this temperature. The system was then refluxed at 295 °C for 1 h and finally

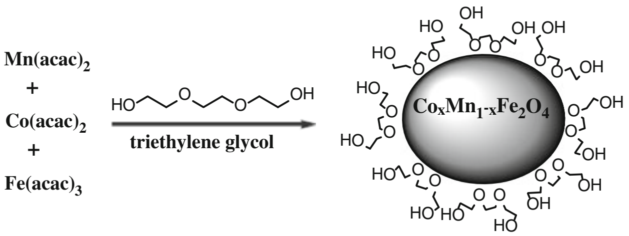

Scheme The synthesis of TEG stabilized $Mn_xCo_{1-x}Fe_2O_4$ NP's

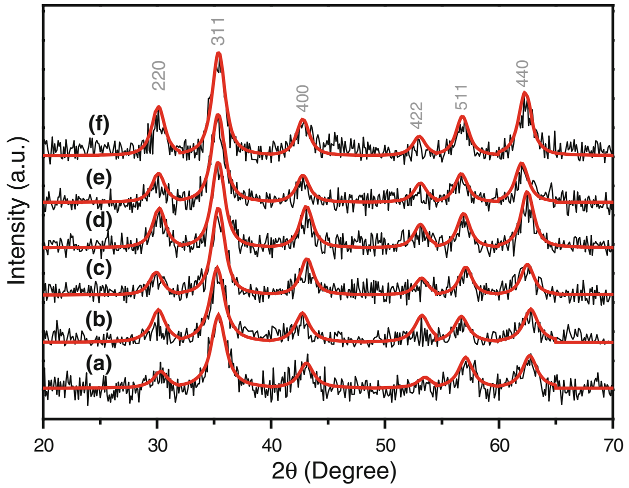

Fig. 1 XRD powder patterns of TEG stabilized $Mn_xCo_{1-x}Fe_2O_4$ NP's *a* x = 0.0, *b* x = 0.2 *c* x = 0.4, *d* x = 0.6, *e* x = 0.8, *f* x = 1.0

Table 1 Crystallite size from XRD and particle size from TEM micrographs for TEG stabilized $Mn_xCo_{1-x}Fe_2O_4$ NP's **a** x = 0.0, **b** x = 0.2 **c** x = 0.4, **d** x = 0.6, **e** x = 0.8, **f** x = 1.0

Sample	Size (nm)	
	XRD (log-normal fit) D_{XRD} □ Av. Size (StD.)	TEM (profile fit) D_{TEM} □ Av. Size (Geo.StD)
a	5.0 ± 3.0	6.8 ± 0.1
b	5.5 ± 1.0	6.5 ± 0.5
c	5.1 ± 2.5	7.1 ± 0.4
d	5.6 ± .10	6.8 ± 0.5
e	5.3 ± 1.1	7.2 ± 0.4
f	5.5 ± 1.2	6.8 ± 0.6

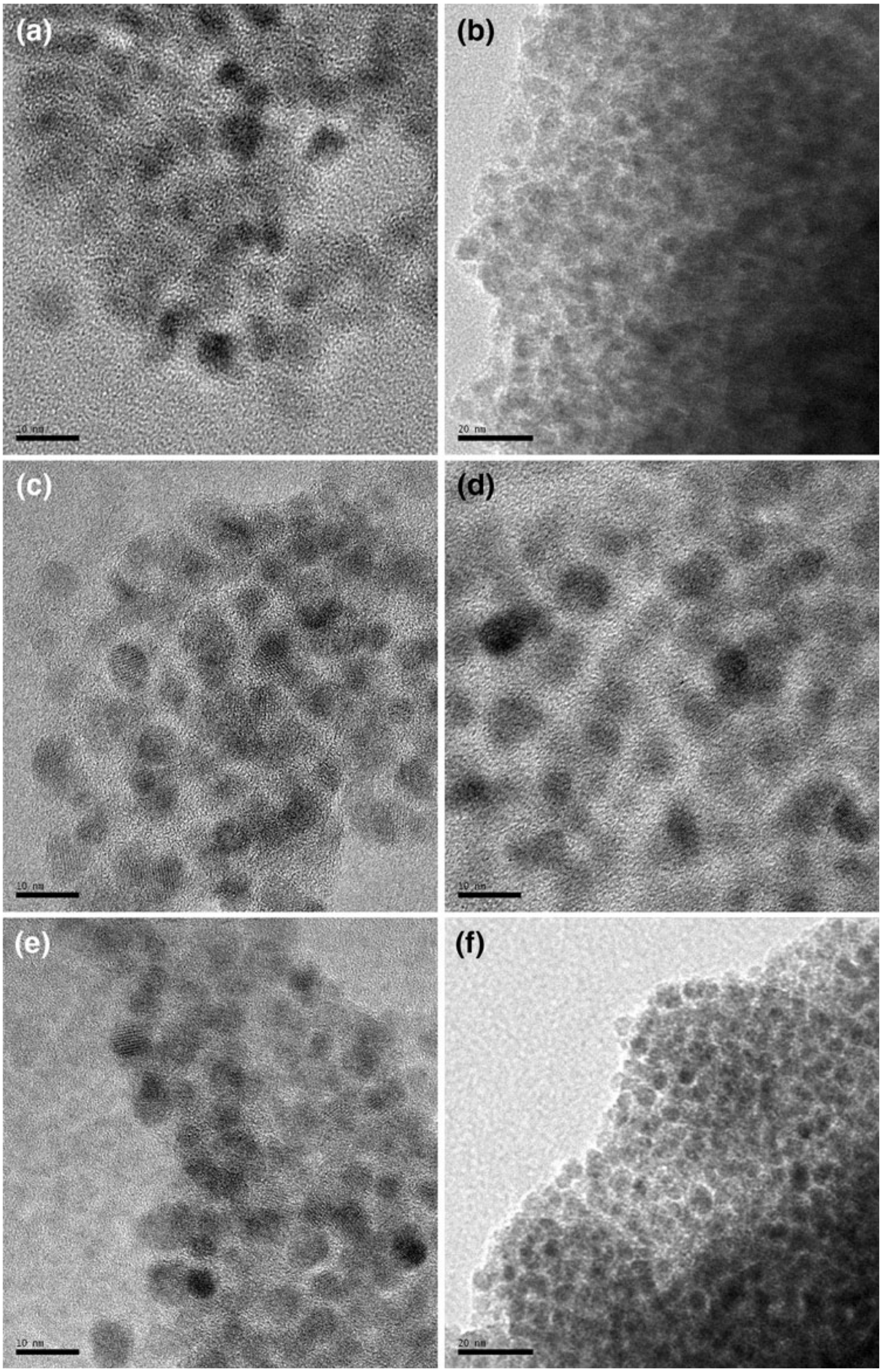

Fig. 2 **a** TEM micrographs of TEG stabilized $Mn_xCo_{1-x}Fe_2O_4$ NP's **a** x = 0.0, **b** x = 0.2, **c** x = 0.4, **d** x = 0.6, **e** x = 0.8, **f** x = 1.0

the black–brown mixture was cooled down to room temperature by removing the heat source. Then, ethanol was added and the solution was centrifuged at 6,000 rpm for 15 min to remove the solvent. The obtained precipitate was washed by ethanol for three times, which could be easily dispersed in water (Scheme).

3 Results and Discussion

3.1 XRD

X-ray powder diffraction patterns of $Mn_xCo_{1-x}Fe_2O_4$ (x = 0, 0.2, 0.4, 0.6, 0.8,1.0) are shown in Fig. 1. XRD

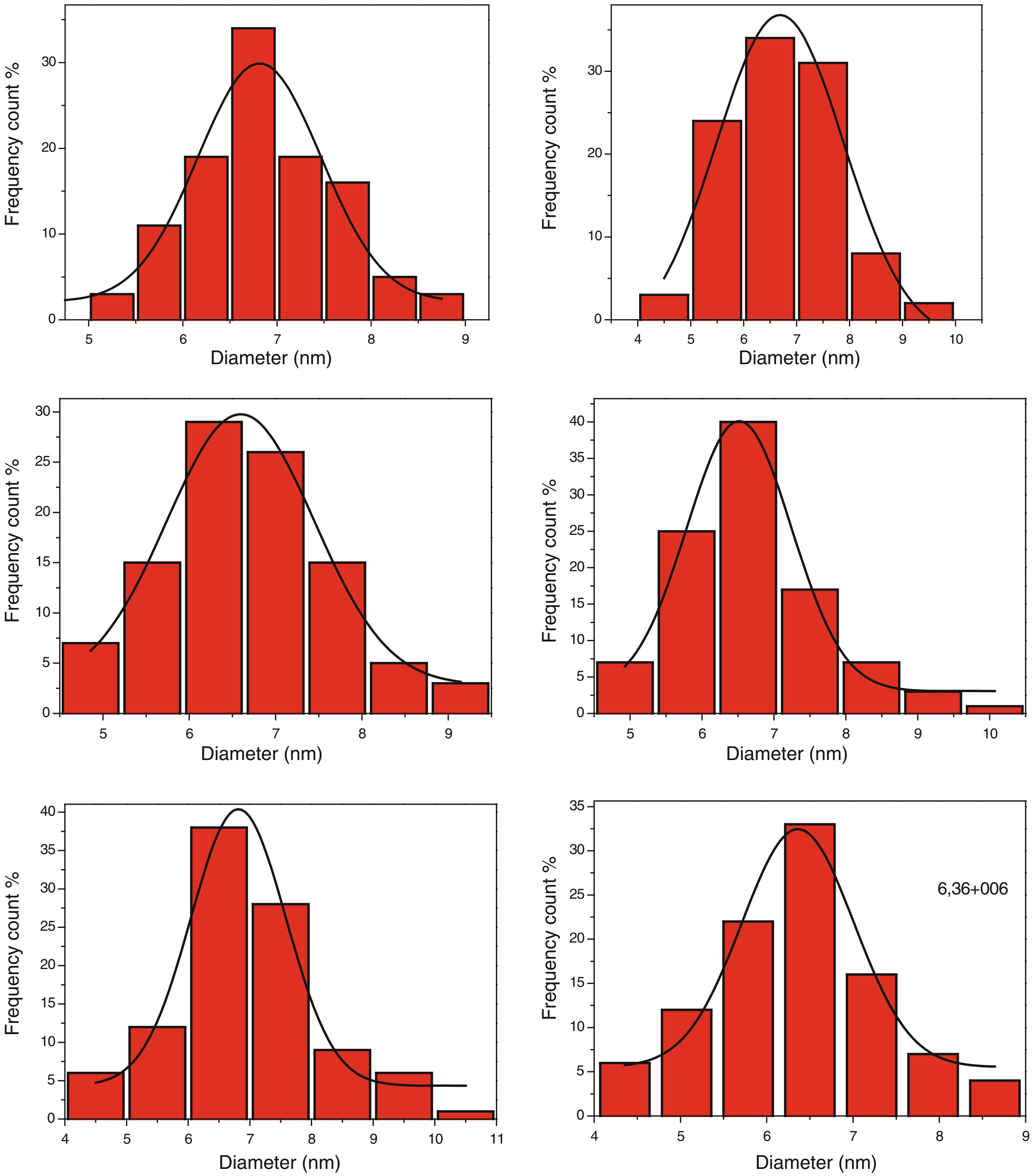

Fig. 3 Particle size distribution histogram of TEG stabilized $Mn_xCo_{1-x}Fe_2O_4$ NP's **a** x = 0.0, **b** x = 0.2 **c** x = 0.4, **d** x = 0.6, **e** x = 0.8, **f** x = 1.0

patterns show the reflection planes (220), (311), (400), (422), (511) and (440) that are indications of the presence of the spinel cubic structure. These diffraction lines corresponding to a cubic, spinel-type and crystalline phase provide clear evidence of the formation of a series of solid solutions between $CoFe_2O_4$ and $MnFe_2O_4$. Mixed spinel ferrites were observed for x = 0.2, 0.4, 0.6, 0.8, whereas for x = 0 pure $CoFe_2O_4$ (JCPDS file No:22-1086), are

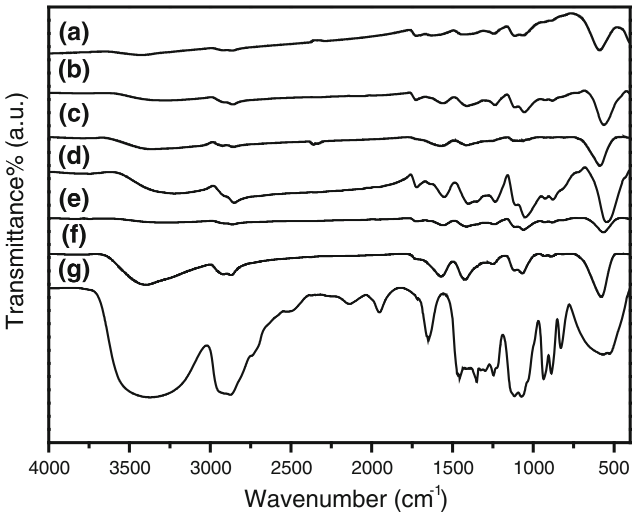

Fig. 4 FT-IR spectra of pure TEG and TEG stabilized $Mn_xCo_{1-x}Fe_2O_4$ NP's

formed. The patterns show also a slight shift in peaks position towards lower d-spacing values with increasing Mn-content in the ferrite. The broadening of the diffraction peaks distinctly indicates the nanocrystalline nature of the materials. The mean size of the samples was estimated from the diffraction pattern by line profile fitting method [15, 16]. The average crystallite sizes, D and s, are summarized in Table 1.

3.2 TEM Analysis

TEM images and particle size distribution diagrams of TREG stabilized $Mn_xCo_{1-x}Fe_2O_4$ nanoparticles with $0 \leq x \leq 1.0$ were presented in Fig. 2 and Fig. 3 respectively. It should be noted that the size of the nanoparticles estimated from the XRD is in good agreement with that obtained from TEM results for all particles. It can be seen that the most of the nanoparticles have roughly spherical shape and are nearly separated from each other. These near-monodisperse nanoparticles show that the magnetic nanoparticles are coated with triethylene glycol (TREG), which is suitable for the biomedical applications.

3.3 FT-IR Analysis

FT-IR analysis further identifies the organic coating in the surface magnetic NP's. Fig. 4 shows the FT-IR spectra of TREG stabilized $Mn_xCo_{1-x}Fe_2O_4$ NP's and pure TREG (Fig. 4a, b). The peaks at ~2,900 and ~2,850 cm^{-1} were assigned to the asymmetric (ν_{as}) and symmetric (ν_s) stretching vibrations of CH_2 of TREG and the peaks at 1,110–1,050 cm^{-1} of C–O–C stretching in spectra of TREG stabilized nanoparticles confirm the presence (or attachment) of TREG on the surface of nanoparticles [11, 17, 18]. And also the presence of the strong metal–oxygen absorption band around 565 cm^{-1}, along with the IR features of TREG molecules for the NP's further supports the stabilizing role of TREG [19].

3.4 Electrical Properties

3.4.1 ac Conductivity

The alternating current (ac) conductivities, $\sigma_{ac}(\omega)$ of TEG stabilized $Mn_xCo_{1-x}Fe_2O_4$ NP's as a function of frequency and temperature are displayed in Fig. 5a–d. Frequency dependent a.c. conductivities, $\sigma_{ac}(\omega)$, have been obtained using the following equation:

$$\sigma'(\omega) = \sigma_{ac}(\omega) = \varepsilon''(\omega)\omega\varepsilon_0 \tag{1}$$

where σ' (ω) is the real part of conductivity, ω(= 2πf) is the angular frequency, ε" is the imaginary part of complex dielectric permittivity (ε*) and ε0(= 8.852×10^{-14} F cm^{-1}) is the vacuum permittivity.

As seen in Fig. 5a–d, the frequency-dependent ac conductivity curves show a general trend for all samples and at all temperatures in the log–log plot. It can be distinguished clearly from the figures that the curves of ac conductivity versus frequency for various temperatures exhibits frequency dependent linear increase at low frequency regime which is assigned to the polarization of the blocking electrodes.

Figure 5a–d shows that the curves of ac conductivities of TEG stabilized-$CoFe_2O_4$ NP's and $Mn_{0.2}Co_{0.8}Fe_2O_4$ NP's increase regularly with temperature and do not show frequency dependency particularly at lower frequency regime whereas it is strongly temperature dependent and it was measured as 7.37×10^{-8} and 1.15×10^{-6} S cm^{-1} for 20 and 120 °C at 1 Hz, respectively.

On the other hand, TEG stabilized $MnFe_2O_4$ and $Mn_{0.8}Co_{0.2}Fe_2O_4$ NP's show both frequency and temperature dependent ac conductivity behavior at low temperatures and frequency zone. The ac conductivities of TEG stabilized nanoparticles at 20 and 120 °C are shown in Table 2. The ac conductivity of TEG stabilized $MnFe_2O_4$ NP's at 1 Hz are found to be 4.56×10^{-6} and 4.71×10^{-5} S cm^{-1} for 20 and 120 °C, respectively while it has a conductivity at the range of 2.33×10^{-5} and 6.61×10^{-5} S cm^{-1} at 1 MHz. TEG stabilized $CoFe_2O_4$ NP's has ac conductivity of 2.31×10^{-10} and 1.15×10^{-8} S cm^{-1} for 20 and 120 °C at 1 Hz, respectively whereas it has conductivity of 2.32×10^{-7} and 4.91×10^{-7} S cm^{-1} at 1 MHz. It has been shown that this phenomenon is a strong clue for ionic conductivity [20].

The comparison with previous study indicates that the conductivities of TEG stabilized $Mn_xCo_{1-x}Fe_2O_4$ NP's are lower than that of pure TEG [21]. This decrease in

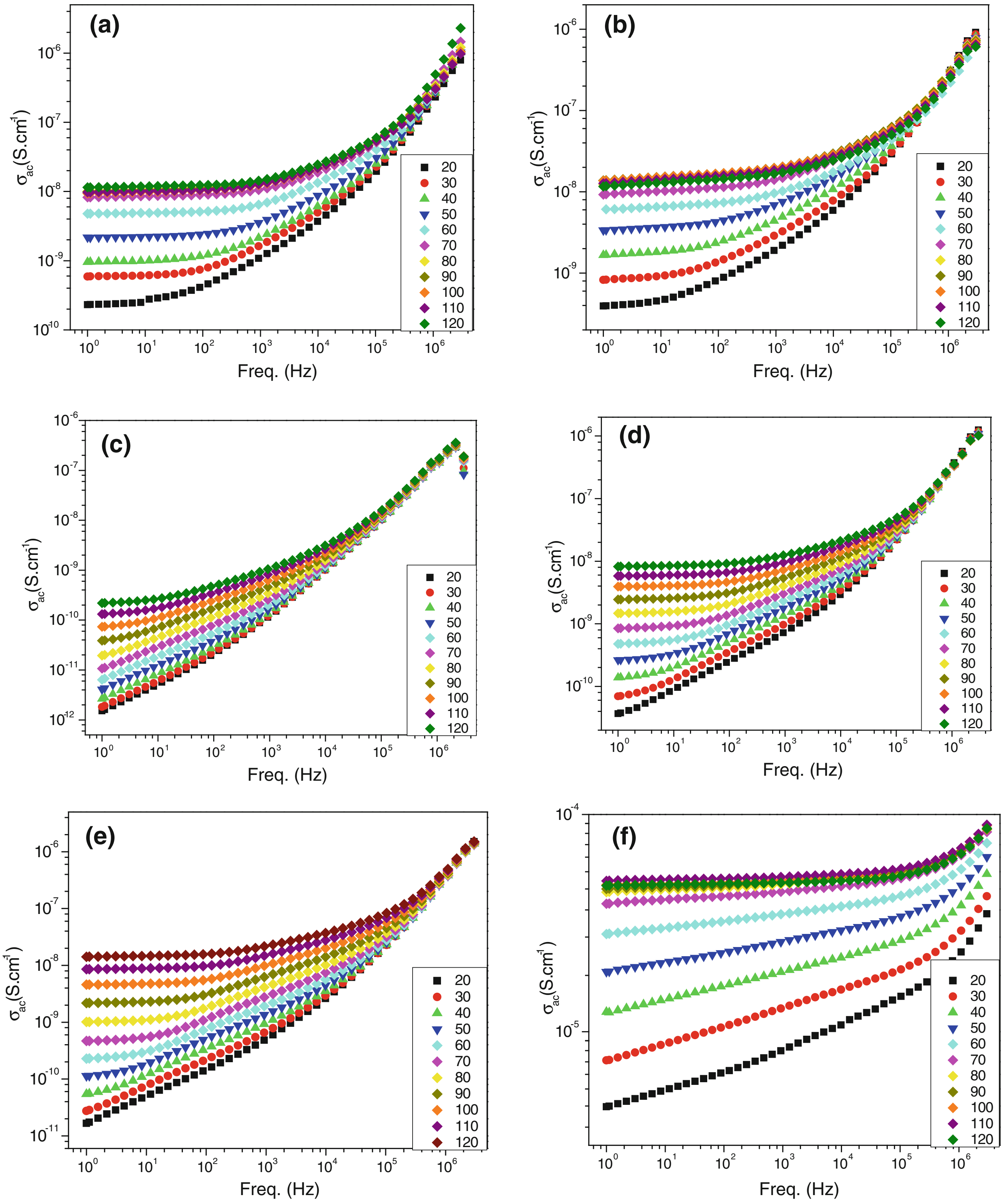

Fig. 5 The variation of ac conductivity of TEG stabilized $Mn_xCo_{1-x}Fe_2O_4$ NP's as a function of frequency and temperature for **a** x = 0.0, **b** x = 0.2, **c** x = 0.4, **d** x = 0.6, **e** x = 0.8, **f** x = 1.0

electrical conductivity with Co and Mn doping may be due to the formation of stable electric bonds between the Co^{2+} and Fe^{2+} ions, which localizes Fe^{2+} charge carriers [22]. As a result, the free surface charge in the medium may decrease due to the surface bonding between TEG and $Mn_xCo_{1-x}Fe_2O_4$ NP's which results in a lower conductivity

Table 2 ac conductivity of TEG stabilized $Mn_xCo_{1-x}Fe_2O_4$ NP's at 20 and 120 °C for 1 Hz and 1 MHz

$Mn_xCo_{1-x}Fe_2O_4$	σ_{ac} (S/cm)			
	1 Hz		1 MHz	
x	20 °C	120 °C	20 °C	120 °C
0.0	2.31×10^{-10}	1.15×10^{-8}	2.32×10^{-7}	4.91×10^{-7}
0.2	3.93×10^{-10}	1.27×10^{-8}	3.13×10^{-7}	2.56×10^{-7}
0.4	1.51×10^{-12}	2.18×10^{-10}	1.47×10^{-7}	1.76×10^{-7}
0.6	3.66×10^{-11}	8.23×10^{-9}	3.76×10^{-7}	3.57×10^{-7}
0.8	1.65×10^{-11}	1.42×10^{-8}	4.16×10^{-7}	4.94×10^{-7}
1.0	4.56×10^{-6}	4.71×10^{-5}	2.33×10^{-5}	6.61×10^{-5}

Table 3 ac conductivity of TEG stabilized $Mn_xCo_{1-x}Fe_2O_4$ NP's at 40 and 80 and 100 °C for 100 kHz

$Mn_xCo_{1-x}Fe_2O_4$	σ_{ac} (S/cm) at 100 kHz		
x	40 °C	80 °C	100 °C
0.0	2.51×10^{-8}	5.6×10^{-8}	5.32×10^{-8}
0.2	3.65×10^{-8}	6.26×10^{-8}	6.0×10^{-8}
0.4	1.05×10^{-8}	1.28×10^{-8}	1.45×10^{-8}
0.6	2.31×10^{-8}	3.21×10^{-8}	3.96×10^{-8}
0.8	2.35×10^{-8}	3.75×10^{-8}	5.60×10^{-8}
1.0	2.64×10^{-5}	5.40×10^{-5}	5.6×10^{-5}

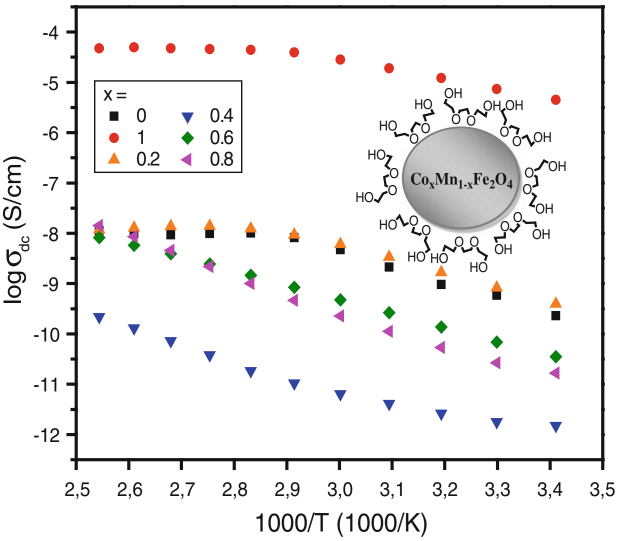

Fig. 6 The variation of dc conductivity of TEG stabilized $Mn_xCo_{1-x}Fe_2O_4$ NP's versus reciprocal temperature

Table 4 The activation energy values of TEG stabilized $Mn_xCo_{1-x}Fe_2O_4$ NP's

$Mn_xCo_{1-x}Fe_2O_4$	Activation energy (eV)	
x	Ea_1	Ea_2
0.0	0.253	0.01
0.2	0.229	0.01
0.4	0.164	0.321
0.6	0.239	–
0.8	0.304	–
1.0	0.153	0.011

Table 5 dc conductivity of TEG stabilized $Mn_xCo_{1-x}Fe_2O_4$ NP's at 20, 80, 100 and 120 °C

$Mn_xCo_{1-x}Fe_2O_4$	log σ_{dc} (S/cm)			
x	20 °C	80 °C	100 °C	120 °C
0.0	−9.64	−7.99	−8.03	−7.94
0.2	−9.41	−7.91	−7.86	−7.93
0.4	−11.83	−10.73	−10.14	−9.67
0.6	−10.45	−8.83	−8.41	−8.08
0.8	−10.78	−8.90	−8.34	−7.85
1.0	−5.35	−4.36	−4.32	−4.32

[23]. The ac conductivities of TEG stabilized $Mn_xCo_{1-x}Fe_2O_4$ NP's versus frequency for various temperatures comprise well developed conductivity plateau regions and it becomes more apparent as temperature increases. The plateaus start at 1 kHz and shift to higher frequencies up to 100 kHz at high temperatures. A significant increase is observed at higher frequencies at all temperature ranges which are assigned to the 'normal' dispersion in polymers and polymer-like materials. The ac conductivities of the composites increase significantly (more than 10^2 times) with temperature until phase transition temperature of about 80 °C. Such a dramatic increase in ac conductivity with temperature can be described by the contribution of the local dynamics, hydrodynamic transport and percolation of the nanocomposites [24]. The $Mn_xCo_{1-x}Fe_2O_4$ NP's may interact with each other leading a percolated path which assists the ionic conduction. It may also indicate the fact that the electrical current flows through both $Mn_xCo_{1-x}Fe_2O_4$ NP's and TEG with the applied temperature which is in agreement with the earlier reports [25].

However, the ac conductivity of samples either starts to decreases slightly or remains constant or slope of increase declines beyond 80 °C (Table 3). The reason for these variations may be explained as formation of random network at low temperatures and then if the temperature is increased, the nanocomposite becomes more organized and exhibits more capacitive behavior and weak frequency response on hopping conduction which results in high electrical conductivity. Since TEG is highly hydroscopic, the reduction in conductivity above 80 °C may be due to the removing of trapped water.

It is clearly observed that all samples displayed a frequency-dependent conductivity at higher frequencies

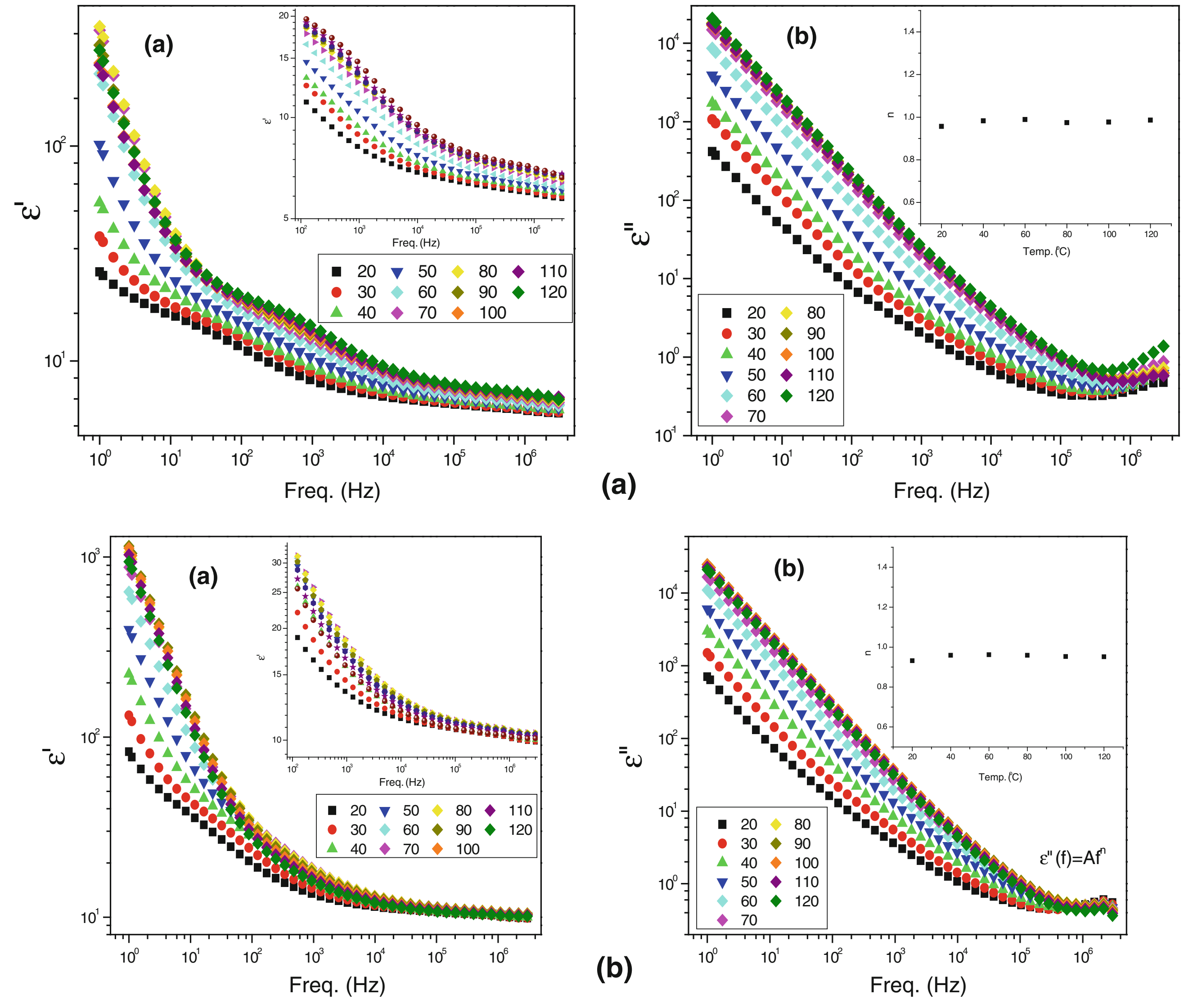

Fig. 7 **a** Real, ε' and **b** imaginary, ε'' parts of permittivity of TEG stabilized $Mn_xCo_{1-x}Fe_2O_4$ NP's as a function of frequency at various temperatures for **a** x = 0.0, **b** x = 0.2, **c** x = 0.4, **d** x = 0.6, **e** x = 0.8, **f** x = 1.0

particularly above 1 MHz. The conductivity above this frequency is independent of temperature and has almost same values while it shows a temperature-dependent behavior at low frequencies. This phenomenon can be considered as a strong evidence for ionic conductivity.

3.4.2 dc Conductivity

The direct current (dc) conductivities of TEG stabilized $Mn_xCo_{1-x}Fe_2O_4$ NP's versus reciprocal temperature are shown in Fig. 6. The frequency independent conductivity is identified with the dc conductivity (σ_{dc}) which was derived from the well-developed plateau region in graphs of σ_{ac} versus *Freq.* by linear fittings. In non- plateau regions, the middle region was fitted linearly to reduce the effect of electrode polarization and dispersion.

The dc conductivity curves exhibits significant influence of temperature on conductivity involving a transition region. The dc curves of nanocomposites for x = 0.6 and 0.8 increase regularly with temperature showing no transition as a result single activation energy is identified whereas the nanocomposites for x = 0, 0.2, 0.4 and 1 show a transition around 80 °C providing two values of the activation energies below and above transition temperature. The conductivity curves at all temperatures can be fitted with Arrhenius equation as follows:

$$\log\sigma_{dc} = \log\sigma_0 - E_a/k_B T \qquad (2)$$

where σ_{dc} is the dc conductivity, σ_0 is the pre-exponential term, E_a is the activation energy, k is the Boltzmann constant (8.617×10^{-5} eV K^{-1}) and T is the temperature in K. Two different activation energies were obtained from

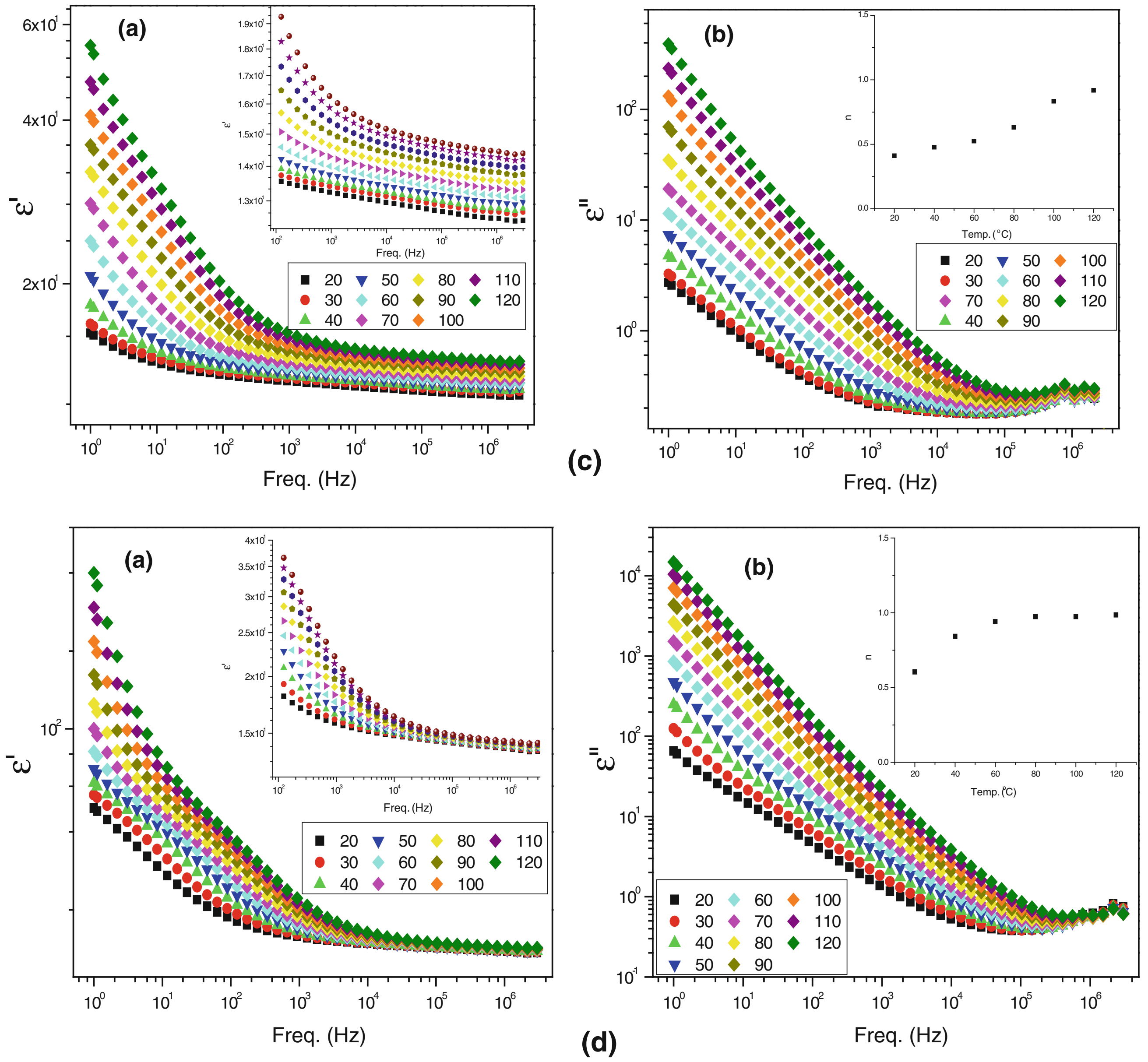

Fig. 7 continued

the slope of the curves for TEG- $Mn_xCo_{1-x}Fe_2O_4$ nanocomposites before and after transition temperature region (Table 4). Such high activation energy values may be the reason of having low dc conductivities. At the same time, the dc conductivity values at temperatures above 80 °C remains constant or slightly shifts to a threshold temperature or increases regularly and this is in consistent with ac conductivities (Table 5).

3.4.3 Permittivity

The frequency and temperature dependent complex permittivity parameters of real ε' and imaginary ε'' parts of TEG stabilized $Mn_xCo_{1-x}Fe_2O_4$ NP's in the frequency range of 1–3.10^6 Hz and temperature range of 20–120 °C are shown in Fig. 7(a–f). It is seen that the real part of permittivity of the nanocomposites exhibits a sharp exponential decay with frequency particularly at high temperatures and at low frequency range while it shows a slight decline at low temperatures including a curvature around 5×10^2 Hz over 80 °C. It is due to the reorganization of nanocomposite at high temperature range as a whole and phase transition when passed through the medium temperature range which is resulted from the relaxation of TEG segments. The real part of dielectric permittivity (ε'), remains almost constant at higher frequency regime.

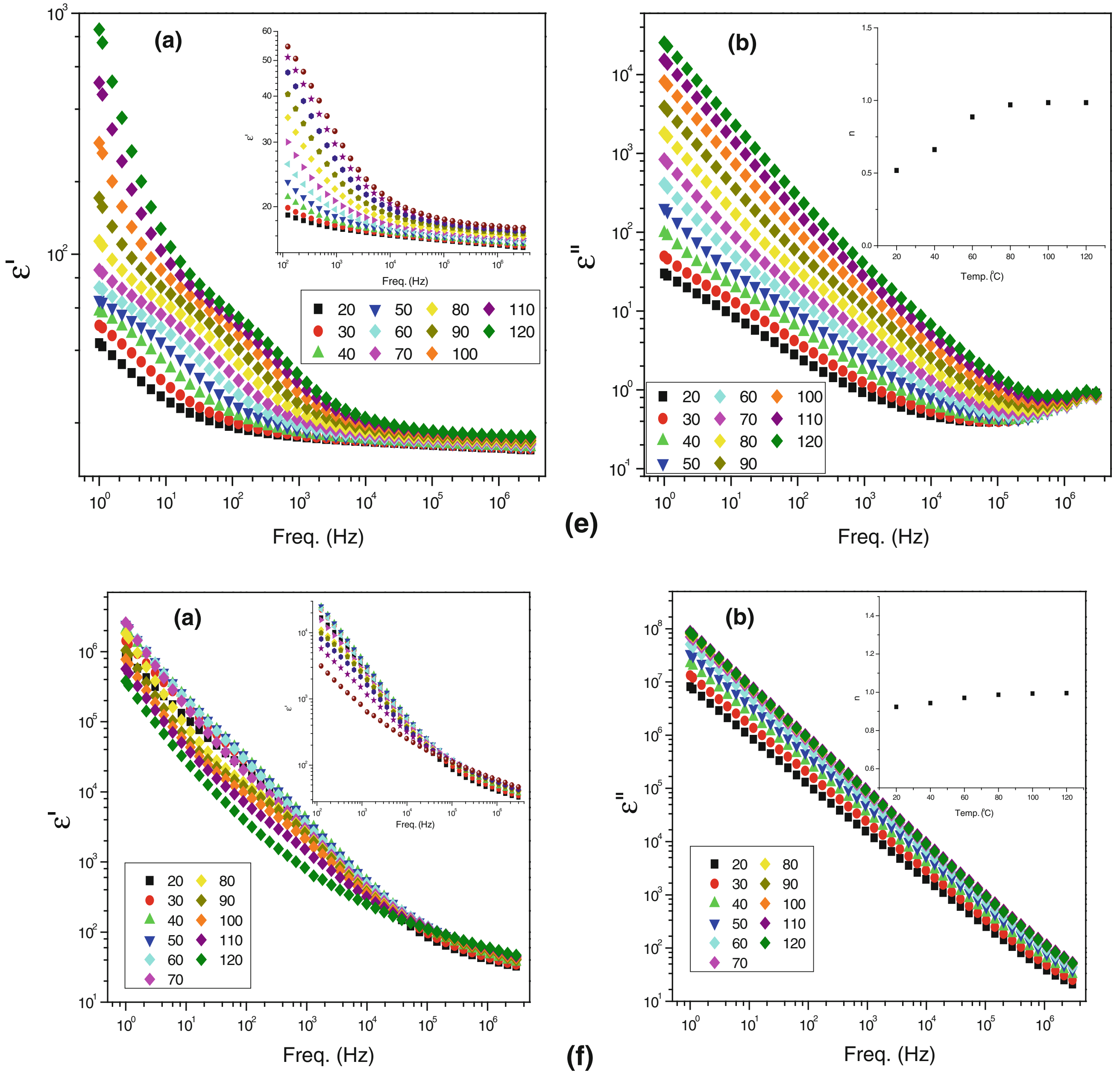

Fig. 7 continued

This indicates that the variation of dielectric constant with frequency showed the presence of material electrode interface polarization processes, which takes place at low frequencies [26]. It is also known that ε′ of polymers, in general, decreases regularly with increasing frequency and TEG stabilized $Mn_xCo_{1-x}Fe_2O_4$ NP's exhibited similar behavior.

The frequency dependent dielectric dispersion curve can be interpreted by Koop's theory which is based on the Maxwell–Wagner model for the inhomogeneous double structure [27, 28]. The inhomogeneous double structure contains the highly conducting grains which are separated by moderately poor conducting grain boundaries. The grain boundaries are found to be more effective at lower frequencies, while grains are more effective at higher frequencies [29]. The conductivity difference between grains and grain boundaries exhibits different resistances which lead to the accumulation of charge carriers in separated boundaries and an increase in dielectric constants.

In general, it can be said that the real part of dielectric permittivity increases with temperature due to the molecular orientation and arrangement [26]. In Fig. 7, it can be seen that ε' of the TEG stabilized $Mn_xCo_{1-x}Fe_2O_4$ NP's increase with temperature owing to the improvement of interfaces between $Mn_xCo_{1-x}Fe_2O_4$ and TEG matrix as

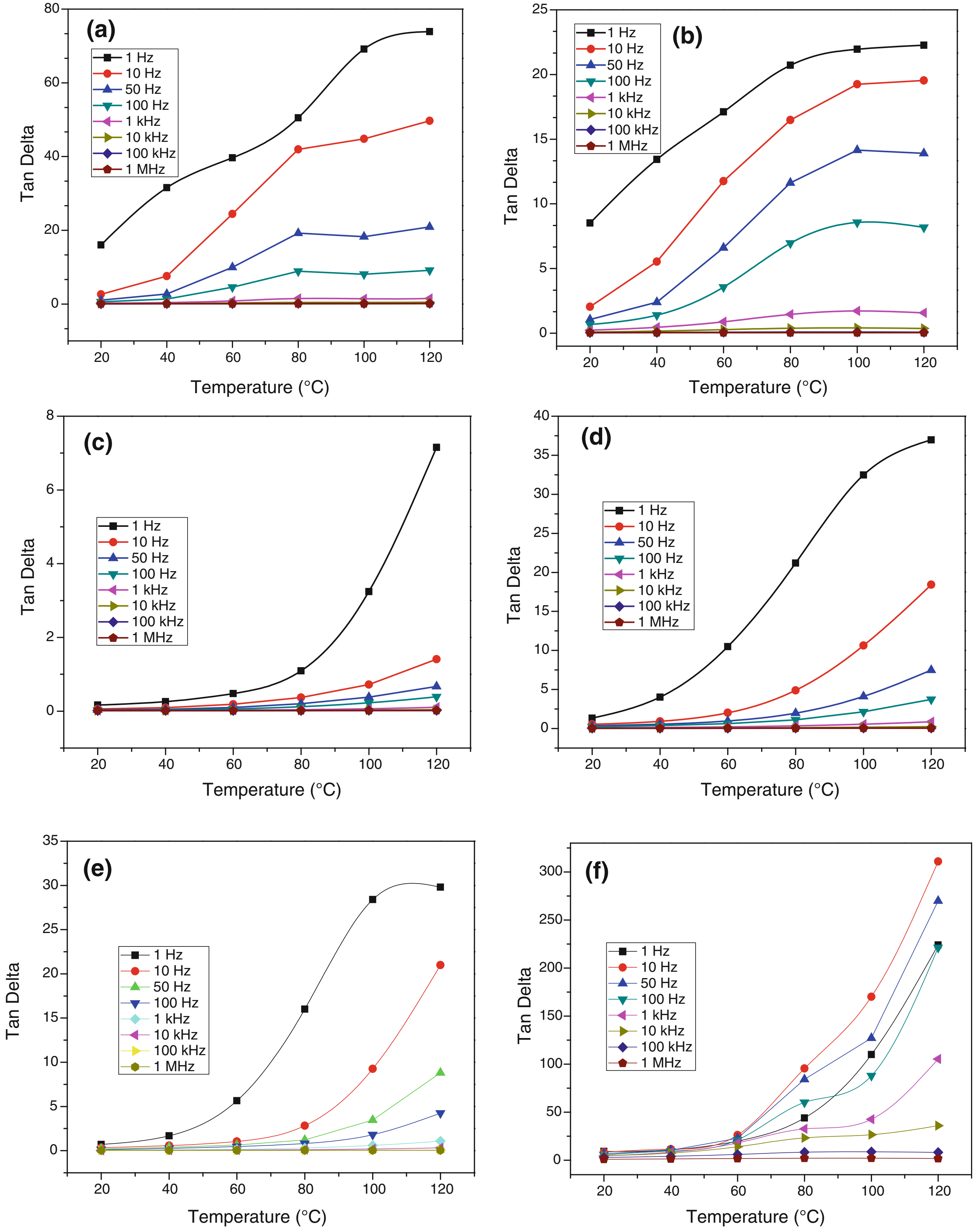

Fig. 8 The tan delta (dissipation factor) variation of TEG stabilized $Mn_xCo_{1-x}Fe_2O_4$ NP's as a function of frequency and temperature for **a** x = 0.0, **b** x = 0.2, **c** x = 0.4, **d** x = 0.6, **e** x = 0.8, **f** x = 1.0

reported in literature [21]. Furthermore, ε' of nanocomposite noticeably increases until the temperature zone between 80 and 100 °C and remains almost the same or slightly lower beyond this temperature zone. It has been reported that chemically bonded TEG stabilized $Mn_xCo_{1-x}Fe_2O_4$ NP's behave as rubber-like and $Mn_xCo_{1-x}Fe_2O_4$ NP's may easily interact with each other providing a percolated path that will facilitate the conduction within this temperature regime [21].

Consequently, the dielectric constant increases generally with increasing temperature as seen in semiconductors. The thermal energy converts the bound charges to the charge carriers. The increase in charge carrier concentration always leads to easy alignment of dipoles in the applied ac electrical field and accordingly increases in dielectric constants. It should be also noted that the mobility of the charge carriers increases by increasing the temperature because of the increase in thermal energy.

Imaginary part of the permittivity (ε''), as a function of frequency for various temperatures has been studied, and related curves are displayed in Fig. 7. The ε'' of the TEG stabilized $Mn_xCo_{1-x}Fe_2O_4$ NP's show a linear decrease with frequency which becomes more considerable at higher temperatures. The grain boundaries are effective at lower frequencies and the grains at higher frequencies as explained above. Therefore, more energy is required for the polarization in the grain boundaries at lower frequencies, results in high energy loss, whereas less energy is required for polarization in the grains and causing small energy loss at high frequencies [23, 30]. Concerning the polarization mechanism, it can be underlined that interface polarization is leading at lower frequencies while other mechanisms such as electronic and ionic exist at higher frequencies [31, 32].

Moreover, the imaginary part of the relative dielectric permittivity of nanocomposite exhibits spectra within the frequency range of measurement which can be analytically well-represented by power laws;

$$\varepsilon''(f) = Af^{-n} \qquad (3)$$

where f is the angular frequency, n is the frequency exponent and A is a temperature independent constant. Frequency exponent (n) values of the nanocomposite for each temperature were calculated from the slopes of log–log graphs. The inset in Fig. 7 shows the variation of the exponent *"n"* with temperature and the correlated power law exponents are in the range of 0.5–1.0 for the nanocomposites. The temperature-dependency of variation of n values of TEG stabilized $Mn_xCo_{1-x}Fe_2O_4$ NP's is a strong evidence for thermally activated polarization mechanism. Accordingly, the imaginary part of permittivity remains unchanged for various temperatures particularly at high frequency range while the exponent "*n*" exhibits slight linear increase with temperatures until certain temperature regime. The curves achieve a constant value after complete reorganization of the TEG stabilized $Mn_xCo_{1-x}Fe_2O_4$ NP's. This expected result is due to the reorganization of nanocomposite at a certain temperature limit which may also indicate that the conduction mechanism is based on ion migration in the applied electric field, the lower n values from the ac measurements can be explained by strong electrode polarization.

3.4.4 *Dissipation Factor (tanδ)*

The dissipation factor (tan δ), which is the ratio of ε″ and ε', of TEG stabilized $Mn_{0.2}Co_{0.8}Fe_2O_4$ NP's was examined as a function of temperature at various frequencies and the graph are shown in Fig. 8(a–d). It is clearly seen from the figures that the frequency at which dissipation factor reaches a maximum shifted towards higher frequencies as the temperature increases. As a general trend, the peaks become broader as frequency increases which may be attributed to the dipoles aligning themselves with the alternating fields as explained before [33]. It has been already reported that the maximum peaks of dissipation factor for pure TEG can be fully observed at lower frequencies below 100 Hz [21]. The disappearance of corresponding maximum peak of dissipation factor for TEG is probably due to the formation of TEG layer on the nanoparticle surface leading a barrier for relaxation. Being out of temperature and frequency range applied in the study may also be another reason for this disappearance. On the other hand, the observed maximum peaks of dissipation factor shifted towards higher frequencies when the temperature increases indicating that relaxation takes places as temperature increases.

4 Conclusion

In summary, monodispersed TEG stabilized $Mn_xCo_{1-x}Fe_2O_4$ NP's were prepared via a one-step polyol reaction in the presence of TEG. The crystallinity of all products was determined with XRD. Crystallite sizes obtained from XRD were close agreement with particle size from TEM for all products. The ac conductivity measurements revealed two trends a temperature dependent behavior at low frequencies and a temperature independent behavior at high frequencies, which is an indication of ionic conductivity. TEG stabilized $Mn_xCo_{1-x}Fe_2O_4$ NP's showed lower conductivity than that of pure TEG since the formation of stable electric bonds between Co^{2+} and Fe^{2+} ions, which localizes Fe^{2+} charge carriers by Co and Mn doping of ferrite nanoparticles resulting in decrease of free surface charges in the medium and as a consequence the composites exhibits lower conductivities. Analysis of dielectric permittivity functions confirms the coupling of the ionic and segmental motions in the nanocomposites. The dielectric constants increased with temperature as expected from semiconductors. It has been observed that the frequency at which dissipation factor reaches a maximum shift towards higher frequencies when the temperature increases. This approach offers a facile route to replace the traditional co-precipitation method for the preparation of magnetic water-soluble magnetic nanoparticles and is expected to be applicable in various biomedical applications.

Acknowledgments This work is supported by Fatih University under BAP grant no P50021104-B.

References

1. A.K.M. Akther Hossain, H. Tabata, T. Kawai, J. Magn. Magn. Mater. **320**, 1157 (2008)
2. R. Arulmurugan, B. Jeyadevan, G. Vaidyanathan, S. Sendhilnathan, J. Magn. Magn. Mater. **288**, 470 (2005)
3. A. Baykal, N. Kasapoğlu, Y. Köseoğlu, M.S. Toprak, H. Bayrakdar, J. Alloys Compd. **464**, 514 (2008)
4. N. Kasapoğlu, A. Baykal, Y. Köseoğlu, M.S. Toprak, Scr. Mater. **57**, 441 (2007)
5. Y. Qu, H. Yang, N. Yang, Y. Fan, H. Zhu, G. Zou, Mater. Lett. **60**, 3548 (2006)
6. R.D.K. Misra, A. Kale, R.S. Srivastava, O.N. Senkov, Mater. Sci. Technol. **19**, 826 (2003)
7. A.K. Gupta, M. Gupta, Biomaterials **26**, 3995 (2005)
8. A. Thangaraja, V. Savitha, K. Jegatheesan, Int. J. Nanotechnol. Appl. **4**, 9 (2010)
9. S. Sun, H. Zeng, D.B. Robinson, S. Raoux, P.M. Rice, S.X. Wang, G. Li, J. Am. Chem. Soc. **126**, 273 (2003)
10. H. Zeng, P.M. Rice, S.X. Wang, S. Sun, J. Am. Chem. Soc. **126**, 11458 (2004)
11. W. Cai, J. Wan, J. Colloid Interface Sci. **305**, 366 (2007)
12. F. Fievet, J.P. Lagier, B. Blin, B. Beaudoin, M. Figlarz, Solid State Ionics **32–33**, 198 (1989)
13. D. Caruntu, G. Caruntu, C.J. O'Connor, Applied physics. J. Phys. D **40**, 5801 (2007)
14. A.K. Sra, T.D. Ewers, R.E. Schaak, Chem. Mater. **17**, 758 (2005)
15. T. Wejrzanowski, R. Pielaszek, A. Opalińska, H. Matysiak, W. Łojkowski, K.J. Kurzydłowski, Analytical expression for diffraction line profile for polydispersive powders, *in 19th Conference on Applied Crystallography*, World Scientific, Kraków, Poland, 2003, p. 43–50
16. T. Wejrzanowski, R. Pielaszek, A. Opalińska, H. Matysiak, W. Łojkowski, K.J. Kurzydłowski, Appl. Surf. Sci. **253**, 204 (2006)
17. J. Giri, T. Sriharsha, S. Asthana, T.K. Gundu Rao, A.K. Nigam, D. Bahadur, J. Magn. Magn. Mater. **293**, 55 (2005)
18. H. Yang, C. Zhang, X. Shi, H. Hu, X. Du, Y. Fang, Y. Ma, H. Wu, S. Yang, Biomaterials **31**, 3667 (2010)
19. H. Deligöz, A. Baykal, E.E. Tanrıverdi, Z. Durmus, M.S. Toprak, Mater. Res. Bull. **47**, 537 (2012)
20. B. Unal, Z. Durmus, H. Kavas, A. Baykal, M.S. Toprak, Mater. Chem. Phys. **123**, 184 (2010)
21. H. Deligöz, A. Baykal, M.S. Toprak, E.E. Tanrıverdi, Z. Durmus, H. Sözeri, Mater. Res. Bull. **48**, 646 (2013)
22. J.S. Ghodake, R.C. Kambale, S.V. Salvi, S.R. Sawant, S.S. Suryavanshi, J. Alloys Compd. **486**, 830 (2009)
23. M.J. Iqbal, B. Ismail, J. Alloys Compd. **501**, 440 (2010)
24. M. Schuster, W.H. Meyer, G. Wegner, H.G. Herz, M. Ise, K.D. Kreuer, J. Maier, Solid State Ionics **145**, 85 (2001)
25. H. Kavas, Z. Durmus, A. Baykal, A. Aslan, A. Bozkurt, M.S. Toprak, J. Non-Cryst, Solids **356**, 484 (2010)
26. S. Ukishima, M. Iijima, M. Sato, Y. Takahashi, E. Fukada, Thin Solid Films **308–309**, 475 (1997)
27. J.C. Maxwell, *A Treatise on Electricity and Magnetism* (Oxford University Press, Oxford, 1873)
28. K.W. Wagner, Ann. Phys. **345**, 817 (1913)
29. K.M. Batoo, S. Kumar, C.G. Lee, Alimuddin, Curr. Appl. Phys. **9**, 1397 (2009)
30. I.M. Afandiyeva, İ. Dökme, Ş. Altındal, M.M. Bülbül, A. Tataroğlu, Microelectron. Eng. **85**, 247 (2008)
31. D.J. Griffiths, *Introduction to electrodynamics* (Prentice Hall, Upper Saddle River, 1999)
32. J.D. Jackson, *Classical electrodynamics* (Wiley, New York, 1999)
33. D.G. Chen, X.G. Tang, J.J. Tong, J.B. Wu, Y.P. Jiang, Q.X. Liu, Solid State Commun. **151**, 1042 (2011)